ISSN 1547-4771, Physics of Particles and Nuclei Letters, 2014, Vol. 11, No. 1, pp. 36–42. © Pleiades Publishing, Ltd., 2014.
Original Russian Text © V.N. Fetisov, 2014, published in Pis'ma v Zhurnal Fizika Elementarnykh Chastits i Atomnogo Yadra, 2014, No. 2(186), pp. 300–311.

METHODS OF PHYSICAL EXPERIMENT

Nuclear and Coulomb Interactions in Coherent Fragmentation of Relativistic Nuclei in a Photoemulsion

V. N. Fetisov

Lebedev Physical Institute, Russian Academy of Sciences, Moscow, Russia
e-mail: fetisov@sci.lebedev.ru

Abstract—The role of the nuclear and Coulomb interactions in coherent fragmentation of relativistic nuclei is discussed with the cluster-model analysis of the experimental data on the fragmentation of ^{7}Li ($P = 3A$ GeV/c) via the ^{3}H + ^{4}He channel in photoemulsion used as an example. The calculated electromagnetic contribution of ~10% to the cross section is not in conflict with the photoemulsion data and the upper estimate of ~40% derived from the earlier measurements of total cross sections for fragmentation of light nuclei using the counter technique. The observed irregularities in the differential cross section for ^{7}Li fragmentation with a separated Coulomb peak at a very small momentum transfer Q are ascribed to the overlap of nuclear diffraction patterns arising from light (C, N, O) and heavy (Ag, Br) photoemulsion nuclei. The predicted diffraction cross sections in the inelastic channel drastically differ from the usual shape of nuclear diffraction in an elastic channel. For pure targets, they have a shape of oscillations with a few peaks of comparable intensity and show strong dependence on the form of the surface nuclear density and radii of the intranuclear cluster and target nucleus. The probability for two-body clustering in ^{7}Li is estimated at about 0.7.

DOI: 10.1134/S1547477114020046

INTRODUCTION

Results of Earlier Investigations into the Problem

It is believed that coherent fragmentation of relativistic nuclei (without destruction of target nuclei) occurs due to nuclear and electromagnetic interactions (often referred to as relativistic Coulomb excitation) in peripheral nucleus–nucleus collisions. Investigations of elastic scattering showed that the nuclear part of the scattering was quite adequately described by the Glauber–Sitenko diffraction theory and that the Coulomb interaction gave rise to a Rutherford peak in the small-angle cross section, which overlaps the main diffraction peak. Inelastic processes with emission of nuclear fragments are much more poorly studied, both because of difficulties in identification and spectrometry of reaction products, especially neutrons, and because of problems in theoretical description of multiparticle final states.

The theory of disintegration of incident nuclei due to the electromagnetic and nuclear interactions in peripheral collisions has long been under development [1]. Most calculations [2–8] deal with the breakup of fast deuterons into a proton and neutron. However, the experimental data for this simplest probe are very limited even at intermediate energies (tens to hundreds of MeV) [9, 10] and are almost absent at relativistic energies. While the description of nuclear interaction is based on the Glauber–Sitenko theory of multiple scattering [1, 5, 6] that allows for Coulomb effects, the microscopic description of the relativistic Coulomb excitation relies on several versions of approximate approaches [11–14]. Verification of these theories in various energy regions is still a pressing problem.

Over 30 years ago a series of experiments on the fragmentation of relativistic ^{12}C, ^{16,18}O, and heavier nuclei was conducted at the Lawrence Berkeley Laboratory (USA) using the counter technique and a wide range of target nuclei in order to find the process of relativistic Coulomb excitation and the relative contributions to the total fragmentation cross sections from the electromagnetic and nuclear interactions [15]. Figure 1 schematically shows fragmentation of the ^{18}O light nucleus at the energy $E = 1.7$ GeV/nucleon on the targets A_T with emission of fragments A_F. To analyze the data, the measured total cross section $\sigma_{tot}(T, F)$ for each target T and fragmentation channel F was written as a sum of nuclear $\sigma_{nucl}(T, F)$ and electromagnetic $\sigma_{em}(T, F)$ cross sections. Nuclear cross sections were determined from the semiempirical relation $\sigma_{nucl}(T, F) = \gamma_T\gamma_F$. This factorized form of the cross section together with the linear $A_T^{1/3}$ dependence of the coefficient γ_T and the experimentally selected parameters for a separated set of fragments and targets with a small contribution from the electromagnetic cross section (weak dependence on Z_T) allowed us to obtain nuclear cross sections for other fragments and targets. The thus-found average cross sections (according to Tables 3 and 4 from [15]) for the strongest nucleon fragmentation channels associated predominantly with the decay of the photonuclear giant

resonance are presented in the table, which gives an idea of the size of the electromagnetic effect on the cross sections for different targets.

It is seen that σ_{em} for neutron channels strongly depend on the target charge almost as Z_T^2. Cross sections for channels with the formation of other fragments only slightly depend on Z_T. These channels with small photonuclear reactions are predominantly due to nuclear interactions.

The last column of the table presents electromagnetic cross sections σ_{ww} calculated by the Weizsäcker–Williams method of virtual photons [16] using the relationships

$$\sigma_{ww} = \int n(\omega)\sigma_\gamma^F(\omega)\frac{d\omega}{\omega}, \quad (1)$$

$$n(\omega) = \frac{2}{\pi}Z_T^2\left(\frac{e^2}{\hbar c}\right)\frac{1}{\beta^2} \times \left[\xi K_0(\xi)K_1(\xi) - \frac{1}{2}\beta^2\xi^2(K_1^2(\xi) - K_0^2(\xi))\right], \quad (2)$$

where $\sigma_\gamma^F(\omega)$ are photonuclear cross sections for formation of fragments A_F, $n(\omega)$ is the number of equivalent photons with energy $\hbar\omega$, K_i are modified Bessel functions, $\beta = v/c$ and γ are ordinary relativistic factors, $\xi = \omega b_{min}/c\gamma\beta$, and b_{min} is the order of magnitude of the sum of the radii of the colliding nuclei $R_I + R_T$. Similar values of σ_{em} and σ_{ww} confirm the electromagnetic origin of σ_{em}. It follows from the above data that the largest ratios $p = \sigma_{em}/\sigma_{nucl}$ are typical of large photonuclear cross sections for processes like the giant resonance predominantly decaying with emission of nucleons. With the ^{18}O fragmentation used as an example, it is shown that this ratio can be as large as ~1.5 for Pb and U targets.

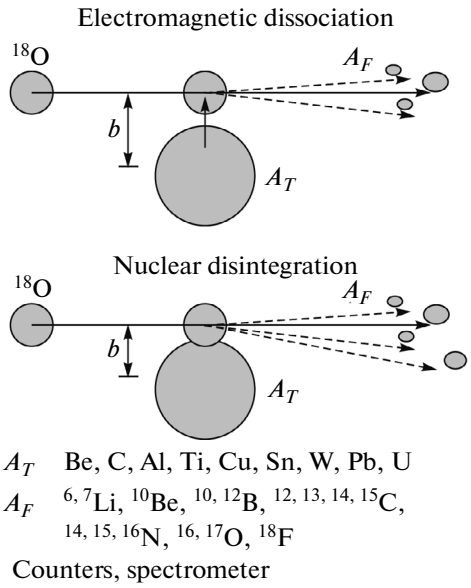

Fig. 1. Coulomb and nuclear fragmentation of the ^{18}O nucleus [15].

Possibilities of the Photoemulsion Method

Particular interest in nuclear structure and contributions from the electromagnetic and strong interaction has been regenerated by measurements of the distributions of events in the transverse momentum transfer Q (in emission angles of fragments) and the corresponding differential cross sections (in mean free path of nuclei) using nuclear photoemulsions bombarded by ordinary and radioactive light nuclei [17–20]. The charged fragments that are to be detected in these reactions are usually protons, deuterons, and ^3H, ^3He, and ^4He nuclei, which largely determine the cluster structure of light projectile nuclei. Electromagnetic dissociation of the projectile nucleus is most likely to arise from interaction with heavy photoemulsion nuclei Br and Ag ($Z_T = 35$ and 47). For the upper estimate of the contribution ratio p in the photoemulsion we can take $p \simeq 0.4$ from the table for the Sn target nucleus, nearest in charge to the Br and Ag nuclei. For lighter projectile nuclei this estimate can be overestimated because of decreasing photoabsorption cross sections in the γ-ray resonance energy region dominating in integral (1) at energies of several GeV/nucleon. In addition, photonuclear cross sections with emission of the lightest nuclei (clusters) are usually much smaller than cross sections with emission of nucleons from the decay of the giant resonance, and for these reactions p can be expected to

Total σ_{tot}, nuclear σ_{nucl}, and electromagnetic σ_{em} and σ_{ww} fragmentation cross sections (mb)

$^{18}O \to A_F$	$_zA_T$	σ_{tot}	σ_{nucl}	σ_{em}	$p=\sigma_{em}/\sigma_{nucl}$	σ_{ww}
$n + {}^{17}O$	$_{22}Ti$	75.3	66.5	8.7	0.13	12.5
	$_{82}Pb$	226.6	90.5	136.0	1.5	135.0
	$_{92}U$	234.0	93.2	140.8	1.51	167.0
$2n + {}^{16}O$	$_{22}Ti$	53.2	46.8	6.4	0.14	5.4
	$_{29}Cu$	59.3	51.1	8.2	0.16	9.0
	$_{50}Sn$	88.7	61.4	27.3	0.44	23.7
	$_{74}W$	111.1	60.5	50.6	0.84	46.8
	$_{82}Pb$	128.7	63.6	65.1	1.02	55.2
	$_{92}U$	139.7	65.5	74.2	1.13	68.1
$p + {}^{17}N$	$_{22}Ti$	40.2	40.7			2.4
	$_{82}Pb$	75.5	55.3	20.2	0.36	23.8
	$_{92}U$	82.0	56.9	25.1	0.44	29.2

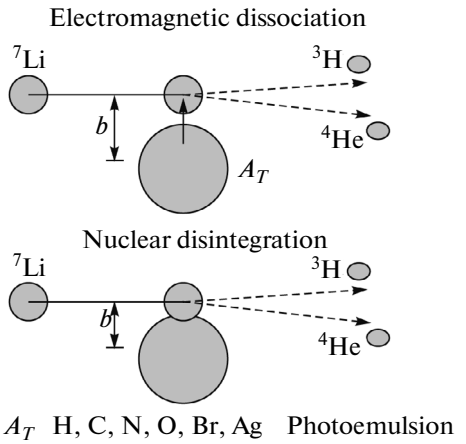

Fig. 2. Coulomb and nuclear fragmentation of the ^{7}Li nucleus [17].

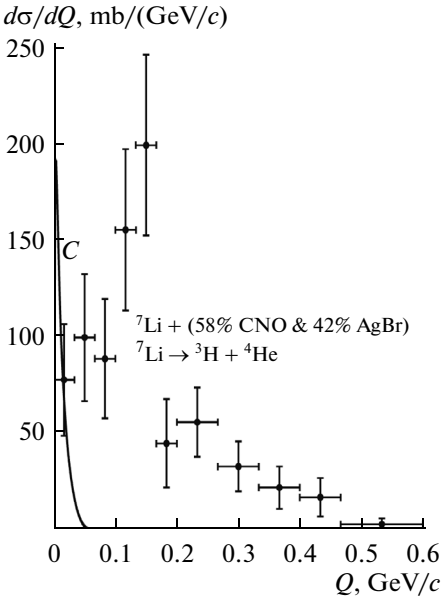

Fig. 3. Differential cross section for ^{7}Li fragmentation in photoemulsion. Points are the experimental data, and curve C is the calculated cross section for the Coulomb dissociation.

decrease. Special calculations are needed to estimate p more accurately, especially for cluster channels.

It is known that the lightest $1p$-shell nuclei, such as ^{6}Li, ^{7}Li, and ^{7}Be, have predominantly a two-cluster structure ^{2}H + ^{4}He, ^{3}H + ^{4}He, and ^{3}He + ^{4}He. Unlike the breakup of the deuteron into a proton and a neutron, fragmentation of the above nuclei into a pair of charged clusters is unambiguously identified in nuclear photoemulsion. Measurements of differential cross sections, unlike experiments on total cross sections, make it possible to reveal Q regions of electromagnetic and nuclear interactions, investigate cross-section behavior features, and estimate the contribution from the interference of these interactions. The next section gives an interpretation of the experimental data on two-cluster fragmentation of ^{7}Li in photoemulsion obtained by Kharlamov's group (High-Energy Physics Department, LPI) [19, 20].

AN EXAMPLE OF ^{7}Li(P = 3 A GeV/c) → ^{3}H + ^{4}He FRAGMENTATION ON PHOTOEMULSION NUCLEI

Experimental study of this process (Fig. 2) is attractive because it can be conveniently interpreted using previously developed theoretical methods, namely,

1. The two-cluster ^{7}Li model with forbidden states [21, 22].

2. The multipole expansion of the electromagnetic interaction between a relativistic nucleus and a target nucleus [13].

3. The Glauber–Sitenko diffraction theory of nuclear interaction in the cluster approximation proposed in [23, 24].

Figure 3 shows the measured differential cross section. Unlike the case in the elastic scattering with the main peak in the cross section at zero Q, in the inelastic channel the peak is seen to shift to the region $Q \simeq$ 0.15 GeV/c. In addition, the behavior of the cross section exhibits irregularities in the interval $Q \leq$ 0.5 GeV/c.

Electromagnetic Dissociation

When calculating cross sections, we use wave functions of two allowed $3P_{3/2}(-2.36$ MeV, ^{7}Li ground state) and $3P_{1/2}(-1.59)$ and six forbidden $0S_{1/2}(-57.4)$, $2S_{1/2}(-15.9)$, $1P_{3/2}(-34.4)$, $1P_{1/2}(-32.3)$, $2D_{5/2}(-13.7)$, and $2D_{3/2}(-11.1)$ bound states in the Woods–Saxon potential with the spin–orbit and Coulomb interaction between the clusters (numbers in parentheses are level energies in MeV; the principal quantum number determines the number of nodes of the radiation function) [25]. Note that this cluster model describes the scattering phases, photodisintegration process, static nuclear properties, and nuclear form factors well [25, 26].

An important assumption in a few developed theories of Coulomb dissociation of relativistic nuclei [11–14] is the smallness of the Coulomb amplitude (stepped behavior) for the impact parameters $b \leq R$, where R is on the order of the sum of the radii of the colliding nuclei. It is assumed that the nuclear disintegration mechanism dominates for these b. At the same time, the microscopic Glauber–Sitenko diffraction theory does not discriminate between the nuclear and Coulomb interaction regions, and the corresponding phases enter into the profile functions on equal terms. The validity of various approximations requires experimental verification.

The cross section for disintegration of ^{7}Li in the Coulomb field was calculated in the Bertulani–Baur formalism using the expansion of the electromagnetic interaction in multipoles for relativistic nuclei. The major contribution to the cross section comes from the $E1$ transitions $3P_{3/2} \to S_{1/2}$, $D_{3/2}$, $D_{5/2}$. Integrating in the initial expression for the cross section over the angular variables of the wave vector $\mathbf{k}$ of the relative motion of the α particle and the tritium nucleus (t) and over the azimuth angle of the vector $\mathbf{Q}$, we obtain

$$\frac{d\sigma_C}{dQ} = \frac{32}{9}\left(\frac{Ze^2}{\hbar v}\right)^2 c_d Q R^2 \times \int_0^\infty \frac{\xi^2}{(\xi^2 + (QR)^2)^2}\left(I_2^2(k) + \frac{1}{2}I_{0,1/2}^2(k)\right)\left(f_1^2 + \frac{1}{\gamma^2}f_0^2\right)k^2 dk. \quad (3)$$

Here functions f_n and radial integrals $I_{l,j}(k)$ for dipole transitions have the form

$$f_n = \xi J_n(QR)K_{n+1}(\xi) - QRJ_{n+1}(QR)K_n(\xi),$$
$$I_{l,j}(k) = \int_0^\infty R_{l,j}(k, r)R_i(r)r^3 dr, \quad (4)$$

where J_n and K_n are the Bessel functions, l and j are the orbital and total moments, and R_i and $R_{l,j}$ are the wave functions of the clusters in the ground state (binding energy $E_b^{\exp} = 2.47$ MeV) and in the continuum. In the integrals $I_{2,j} = I_2$ the small difference of the $D_{3/2}$ and $D_{5/2}$ states is ignored. The functions $R_{l,j}(k, r)$ are normalized in such a way that they pass into spherical Bessel functions when the interaction is switched off. In (3) Z is the number of protons in the target nucleus, v is the ^{7}Li velocity, the coefficient $c_d = (Z_1\beta_1 - Z_2\beta_2)^2$ (where $\beta_{1(2)} = m_{2(1)}/(m_1 + m_2)$, m_i are masses of clusters) governs the dipole moment of the cluster system, $\gamma = (1 - (v/c)^2)^{-1/2}$, $\xi = (\omega R)/(\gamma v)$, $\hbar\omega = E_b + (\hbar k)^2/(2\mu_{\alpha t})$, and $\mu_{\alpha t}$ is the reduced mass of α and t. The calculations are performed with the averages $\bar{R} = 5.0$ fm, $\bar{Z} = 7$ (CNO) and $\bar{R} = 8.1$ fm, $\bar{Z} = 41$ (AgBr). Curve C in Fig. 3 shows the Q dependence of the cross section in a very narrow interval $Q \le 50$ MeV/c with a peak at $Q \simeq 3.5$ MeV/c. For the photoemulsion (58% CNO + 42% AgBr) the calculated total cross section σ_C is 4 mb. The small σ_C and the fact that only 7% of events fall within the expected Coulomb disintegration region indicate that the contribution from nuclear fragmentation has to be considered.

Nuclear Diffraction

According to the Akhiezer–Glauber–Sitenko formalism [6] developed in [23, 24] to fit the diffraction scattering of two-cluster nuclei, the process cross section is determined by the matrix elements of the combination of profile functions $\omega(b)$

$$\omega_\alpha(b_\alpha) + \omega_t(b_t) - \omega_\alpha(b_\alpha)\omega_t(b_t),$$
$$\text{where } \omega_i(b) = 1 - \exp(i\chi_i(b)). \quad (5)$$

The first two terms in (5), which correspond to the impulse approximation, make the major contribution to the cross section

$$\frac{d\sigma_N}{dQ} = A\left(1 + I_0(Q) - \frac{3}{2}\sum_{lj,L}\left(I_L^{lj}(\beta_1 Q) + (-1)^L I_L^{lj}(\beta_2 Q)\right)^2 \times \hat{\hat{lj}}(10l0|L0)^2\left\{\begin{array}{ccc} j & l & 1/2 \\ 1 & 3/2 & L \end{array}\right\}^2\right), \quad (6)$$

$$\frac{A}{4\pi Q} = \left|\int_0^\infty \omega(b)J_0(Qb)bdb\right|^2, \quad I_0(q) = \int_0^\infty j_0(qr)R_i^2 r^2 dr,$$
$$I_L^{lj}(q) = \int_0^\infty j_L(qr)R_{lj}R_i r^2 dr. \quad (7)$$

Expression (6) was obtained using the completeness of the cluster Hamiltonian states, which allowed integration over continuum states to be eliminated and the cross sections to be expressed in terms of the matrix elements over all (both allowed and forbidden) bound (l, j) states. In (6) the factors following the factor $\hat{\hat{lj}} = (2l + 1)(2j + 1)$ are the squares of the Clebsch–Gordan coefficient and the 6j symbol. As the calculations show, the alternating-sign contribution from the third term in (5), which corresponds to the collision of two clusters with the target nucleus (eclipse terms), affects the cross section at a level of no more than 1 to 2%.

Before calculating profile functions with realistic densities of clusters and target nuclei, we investigated the effect of nuclear skin diffuseness on the differential cross sections. In the approximation of the sharp nuclear boundary the profile function $\omega(b)$ has a stepped shape [6] with the width R on the order of the sum of radii of colliding nuclei and the cross section is proportional to the factor $J_1^2(QR)$. The diffraction cross section for the Ag and Br targets is shown in Fig. 4a. A large number of cross-section oscillations are seen in the Q interval, which is much greater than the observed interval $Q \lesssim 0.5$ GeV/c, and the total cross section (250 mb) is several times larger than its measured value ((31 ± 4) mb). At the same time, when the Fermi-shape profile function with the standard diffuseness parameter $a \simeq 0.5$ fm is used, the number of oscillations sharply drops, the cross section becomes several times smaller, and the maximum boundary $Q^{\max}$, as is seen in Fig. 4b, is close to the observed one. Note that the effect of nuclear surface diffuseness on the total cross section for the diffraction disintegration of the deuteron was studied earlier in

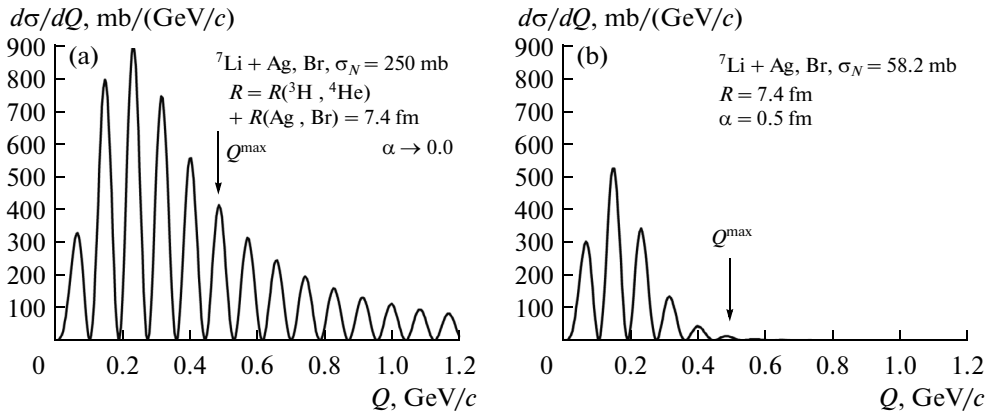

Fig. 4. Diffraction cross sections calculated with the stepped shape of the profile function (a) and the phenomenological Fermi shape of the profile function (b) for the cluster–target nucleus system.

[28], where it was shown that the cross section for that process drastically decreased with increasing diffuseness parameter (Sitenko–Tartakovskii effect).

Qualitatively more accurate results are obtained with the phase functions $\chi_i(b)$, which describe the collisions of nuclei with mass numbers A_1 and A_2, which are calculated in the optical limit of the Glauber–Sitenko model using the formulas for convolution of the nuclear form factors $S_{A_i}(q)$ and the NN amplitude [29]

$$i\chi(b) = -\frac{A_1A_2\sigma_N}{8\pi^2}(1-i\rho) \times \int \exp\left(-i\mathbf{qb} - \frac{a_Nq^2}{2}\right) K(q)S_{A_1}S_{A_2}d^2q. \quad (8)$$

For (α, t) clusters and 1p-shell nuclei form factors were calculated with the density distribution in the oscillator shell model with a correction for the motion of the center of mass due to the factor $K(q)$. For heavy nuclei (Ag, Br) the Fermi density distribution was taken into account. Parameters of the oscillator model ($\hbar\omega$) and the Fermi distribution (R and a) were reconciled in a standard way [31, 32] with the experimental root-mean-square nuclear radii [32] $\bar{r}_t = 1.7$ fm, $\bar{r}_\alpha = 1.67$ fm, $\bar{r}_{CNO} = 2.54$ fm, $\bar{r}_{Br} = 5.1$ fm, and $\bar{r}_{Ag} = 5.62$ fm. The adopted values of the NN interaction parameters are $\sigma_N = 43$ mb, $\rho = -0.35$, and $a_N = 0.242$ fm^2 [31]. Since there is only slight difference between ω_α and ω_t, we use their half-sum as the function $\omega(b)$ for the chosen target nucleus. The real and imaginary parts of $\omega(b)$ for the light and heavy emulsion nuclei are shown in Fig. 5.

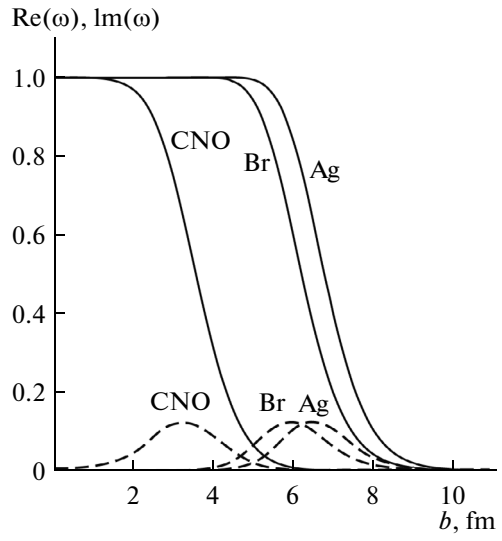

Fig. 5. Real Re(ω) (solid lines) and imaginary Im(ω) (dashed lines) parts of the profile functions.

The calculated differential cross sections for the light (C, N, O) and heavy (Br, Ag) target nuclei are shown separately in Fig. 6. These cross sections drastically differ from the usual diffraction elastic scattering cross sections by having no peak at zero Q, which results from orthogonality of the bound cluster state in ^{7}Li and the cluster states in the continuous spectrum. In addition, while in elastic scattering the intensity of diffraction oscillations following the main peak decreases by orders of magnitude, in inelastic scattering the intensities of oscillations are comparable in magnitude. The number and intensity of peaks mainly depend on the extension (width) of the real part of the profile function in the variable b, which is close to the sum of the radii of the intranuclear cluster and the target nucleus: the wider the profile function, the larger oscillations in the cross section, with the peaks shifting to smaller Q. The difference of the cross sections on the pure nuclei C, N, O and Ag, Br is due to the large difference in width between the profile functions (see Fig. 5) caused by greatly different radii of the above target nuclei in the emulsion: the radii of the heavy nuclei are about twice as large as the radii of the light nuclei. Note the results reported in [20],

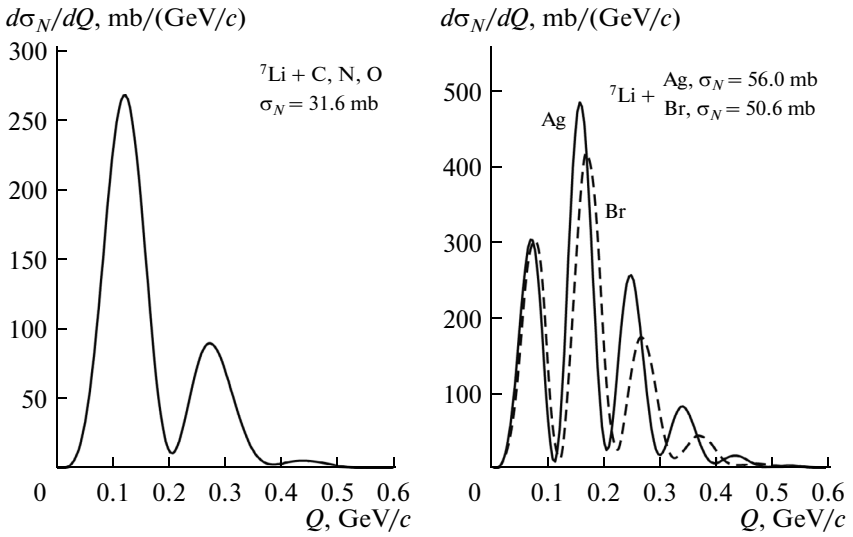

Fig. 6. Diffraction cross sections calculated with the realistic density distributions of the cluster and the target nucleus.

where differential cross sections for the two-cluster ^{7}Li fragmentation on photoemulsion protons were measured. The peak of the cross section on the proton turned out to be shifted to larger Q as compared with the peak of the cross section for the C, N, and O nuclei (see Fig. 6). This shift can be qualitatively explained by a narrower (on the order of the cluster radius) width of the profile function for the cluster–proton system in comparison with the width of the profile function for the cluster–nucleus system. The calculations of the cross section for fragmentation on the proton will be published in a separate paper.

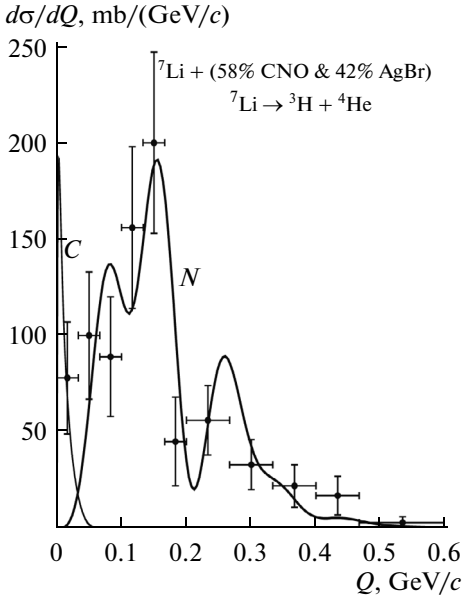

Fig. 7. Experimental (points) and theoretical (curves) data on the cross sections for the Coulomb (C) and nuclear diffraction (N) disintegration of ^{7}Li.

The differential process cross section for the photoemulsion shown in Fig. 7 was obtained by the addition of the two diffraction patterns presented in Fig. 6 with allowance for the percentage of the light and heavy nuclei. The theoretical cross section reproduces the irregularities vaguely manifested in the experimental cross section. As is evident from Fig. 7, the Coulomb and nuclear cross sections are noticeably separated with a small overlap area, which points to the smallness of the contribution from the interference of the Coulomb and nuclear interactions to the fragmentation process under discussion. Note that the calculated total cross section value 44.7 mb is larger than its experimental value (31 ± 4) mb. The curves in Fig. 7 are normalized to the measured total cross section with the coefficient $k = 7$, which can be interpreted as the probability of two-body clustering ^{3}H + ^{4}He in the wave function of the ^{7}Li nucleus.

CONCLUSIONS

Among a variety of nuclear fragmentation processes in peripheral collisions of relativistic nuclei, those that are easier to analyze theoretically are of great importance. These are first of all reactions with two nuclei in the final state. An example of a reaction like this, apart from the breakup of a deuteron into a proton and a neutron, for which there are almost no data at relativistic energies, is fragmentation of ^{7}Li via the ^{3}H + ^{4}He channel, whose differential cross section was measured by Kharlamov's group using the nuclear photoemulsion technique. In the above analysis we tried to emphasize those aspects of nuclear reaction mechanisms and nuclear structure that are responsible for the observed features of the process.

The calculated cross section for the relativistic Coulomb dissociation of the ^{7}Li nucleus is mostly within a narrow interval of small Q ($Q \leq 50$ MeV/c) and is about 10% of the total cross section. This result does not contradict the upper estimate of the ratio $p = \sigma_{em}/\sigma_{nucl} \simeq 0.4$ derived from the LBL data on total cross sections.

The observed irregularities in the differential cross section arise from the overlap of different diffraction patterns from two groups of photoemulsion nuclei C, N, O and Ag, Br with radii that are almost a factor of two different. It can be stated that the photoemulsion technique yields the visual diffraction pattern of a nuclear inelastic process.

The predicted diffraction cross sections on pure target nuclei have the shape of oscillations that are comparable in intensity, which is sharply different from the usual shape of the elastic scattering cross section with the main peak at the zero momentum. The width of the interval Q^{max} where oscillations are still noticeable, their number, and cross sections values at peaks strongly depend on diffuseness of the surface layer of the colliding nuclei. Reasonable cross sections and interval widths ($Q \leq 0.5$ GeV/c) are obtained with the Fermi density distribution.

The analysis shows that the two-cluster model of a nucleus with forbidden states, which underlies the calculations, is quite adequate. Normalization of the calculated total cross section to the experimental value requires introduction of the coefficient $k = 0.7$, which can be interpreted as the probability of the two-cluster state ^{3}H + ^{4}He in the ^{7}Li nucleus.

Despite the rather low measurement statistics that are typical of the photoemulsion technique, the available experimental data, as their analysis shows, are relevant to important aspects of collision physics and the structure of relativistic nuclei. These results can be a guideline for new experiments on the study of relativistic fragmentation on pure target nuclei using other methods that allow higher statistics.

ACKNOWLEDGMENTS

The author is grateful to S.P. Kharlamov, N.G. Peresad'ko, and Yu.A. Aleksandrov, who initiated this work, for numerous discussions of the problems of studying collisions of relativistic nucleus using the nuclear photoemulsion technique. The work was supported by the Russian Foundation for Basic Research, projects 07-02-00871-a and 12-02-01238-a.

REFERENCES

1. A. G. Sitenko, *Theory of Nuclear Reactions*, (Energoatomizdat, Moscow,1983) [in Russian].
2. S. M. Dancoff, Phys. Rev. **72**, 1017 (1947).
3. L. N. Rozentsveig and A. G. Sitenko, Zh. Eksp. Teor. Fiz. **30**, 427 (1950).
4. E. L. Feinberg, Zh. Eksp. Teor. Fiz. **29**, 115 (1955).
5. R. J. Glauber, Phys. Rev. **99**, 1515 (1955).
6. A. I. Akhiezer and A. G. Sitenko, Phys. Rev. **106**, 1236 (1957).
7. M. V. Evlanov and A. M. Sokolov, *Diffraction Interaction of Hadrons with Nuclei*, Ed. by A. I. Akhiezer (Naukova dumka, Kiev, 1987) [in Russian].
8. M. V. Evlanov, A. M. Sokolov, and V. K. Tartakovskii, Phys. At. Nucl. **66**, 253 (2003).
9. N. Matsuoka et al., Nucl. Phys. A **391**, 357 (1982).
10. H. Okamura et al., Phys. Rev. C **58**, 2180 (1998).
11. A. Winther and K. Alder, Nucl. Phys. A **319**, 518 (1979).
12. R. Jäckle and H. Pilkuhn, Nucl. Phys. A **247**, 521 (1975).
13. C. A. Bertulani and G. Baur, Phys. Rep. **163**, 299 (1988).
14. B. V. Carlson, L. F. Canto, and M. S. Hussein, Phys. Rev. C **72**, 041603-1 (2005).
15. H. H. Heckman and P. J. Lindstrom, Phys. Rev. Lett. **37**, 56 (1976); G. D. Westfall et al., Phys. Rev. C. **19**, 1309 (1979); D. L. Olson et al., Phys. Rev. C. **24**, 1529 (1981); M. T. Mercier et al, Phys. Rev. C **33**, 1655 (1986).
16. J. D. Jackson, *Classical Electrodynamics*, 2nd ed. (Wiley, New York, 1975).
17. M. I. Adamovich et al., J. Phys. G **30**, 1479 (2004).
18. P. I. Zarubin, *III Cherenkov Readings: New Methods in Experimental Nuclear Physics and Particle Physics, Moscow, FIAN, 6 April 2010. Collected Papers* (FIAN, Moscow, 2010), p. 49 [inRussian]; The BECQUEREL Project. http://becquerel.jinr.ru.
19. N. G. Peresad'ko, V. N. Fetisov, Yu. A. Aleksandrov, S. G. Gerasimov, V. A. Dronov, V. G. Larionova, E. I. Tamm, and S. P. Kharlamov, JETP Lett. **88**, 75 (2008).
20. N. G. Peresadko, Yu. A. Alexandrov, S. G. Gerasimov, V. A. Dronov, V. G. Larionova, A. V. Pisetskaya, E. I. Tamm, V. N. Fetisov, S. P. Kharlamov, and L. N. Shesterkina, Phys. At. Nucl. **73**, 1942 (2010).
21. V. G. Neudachin and Yu. F. Smirnov, in *Current Problems of Optics and Nuclear Physics: Collected Works* (Kiev, 1974), p. 225 [in Russian].
22. V. I. Kukulin, V. G. Neudachin, and Yu. F. Smirnov, Fiz. Elem. Chastits At. Yadra **10**, 1236 (1979).
23. M. V. Evlanov, A. M. Sokolov, and V. K. Tartakovskii, Phys. At. Nucl. **59**, 647 (1996).
24. V. V. Davidovskii, M. V. Evlanov, and V. K. Tartakovskii, Phys. At. Nucl. **69**, 230 (2006).
25. S. B. Dubovichenko and M. A. Zhusupov, Izv. Akad. Nauk Kaz. SSR , Ser. Fiz.–Mat., No. 4, 44 (1983).
26. N. A. Burkova, K. A. Zhaksybekova, and M. A. Zhusupov, Phys. Part. Nucl. **36**, 427 (2005).
27. C. A. Bertulani and G. Baur, Nucl. Phys. A **442**, 739 (1985).
28. A. G. Sitenko and V. K. Tartakovskii, Ukr. Fiz. Zh. **6**, 12 (1961).
29. V. Franco and A. Tekou, Phys. Rev. C **16**, 658 (1977).
30. L. J. Tassie and F. C. Barker, Phys. Rev. **111**, 940 (1958).
31. V. Franco, Phys. Rev. C **6**, 748 (1972).
32. R. C. Barrett and D. F. Jackson, *Nuclear Size and Structure* (Clarendon Press, Oxford, 1977).

Translated by M. Potapov